Ultrastructural Imaging of *Salmonella*–Host Interactions Using Super-resolution Correlative Light-Electron Microscopy of Bioorthogonal Pathogens

Daphne M. van Elsland[+],[a, b] Sílvia Pujals[+],[c] Thomas Bakkum[+],[a] Erik Bos,[d]
Nikolaos Oikonomeas-Koppasis,[a] Ilana Berlin,[b] Jacques Neefjes,[b] Annemarie H. Meijer,[e]
Abraham J. Koster,*[d] Lorenzo Albertazzi,*[c, f] and Sander I. van Kasteren*[a]

The imaging of intracellular pathogens inside host cells is complicated by the low resolution and sensitivity of fluorescence microscopy and by the lack of ultrastructural information to visualize the pathogens. Herein, we present a new method to visualize these pathogens during infection that circumvents these problems: by using a metabolic hijacking approach to bioorthogonally label the intracellular pathogen *Salmonella* Typhimurium and by using these bioorthogonal groups to introduce fluorophores compatible with stochastic optical reconstruction microscopy (STORM) and placing this in a correlative light electron microscopy (CLEM) workflow, the pathogen can be imaged within its host cell context Typhimurium with a resolution of 20 nm. This STORM-CLEM approach thus presents a new approach to understand these pathogens during infection.

Introduction

The rise of antibiotic resistance is one of the major threats to global health. One class of pathogens proving particularly troublesome in this regard is intracellular bacteria. These thwart immune detection by residing and replicating inside host-cell phagosomes.[1] Through secretion of factors that manipulate phagosomal maturation, they ensure their intracellular survival, despite an extensive arsenal of defence mechanisms deployed by the mammalian host.[2] It is, therefore, of utmost importance to understand bacterium–host interactions at the cellular and molecular levels. Bioorthogonal chemistry has proven to be a major breakthrough technique to study these host–pathogen interactions. Through hijacking the biosynthetic machinery of the cell wall with biorthogonal analogues of D-Ala[3] or trehalose analogues,[4] intracellular pathogens have been visualized selectively within host-cell phagosomes. Bioorthogonal non-canonical amino acid tagging (BONCAT[5])—the incorporation of bioorthogonal amino acids into a target cell proteome—has also proven valuable in this context, for example, to image bacterial protein synthesis or retrieve pathogenic proteins secreted into the host cytosol by *Yersinia enterocolitica*,[6] *Salmonella* Typhimurium,[7] *Escherichia coli*,[8] and *Mycobacterium smegmatis*.[9] However, these labelling approaches either require the mutant tRNA/tRNA synthetase pair specific for the bioorthogonal methionine, phenylalanine, or norleucine analogues to be introduced into the pathogen to achieve incorporation of the desired groups or suffer from low sensitivity.[10]

[a] Dr. D. M. van Elsland,[+] T. Bakkum,[+] N. Oikonomeas-Koppasis,
Dr. S. I. van Kasteren
Leiden Institute of Chemistry and
The Institute for Chemical Immunology, Leiden University
Einsteinweg 55, 2333 CC Leiden (The Netherlands)
E-mail: s.i.van.kasteren@chem.leidenuniv.nl

[b] Dr. D. M. van Elsland,[+] Dr. I. Berlin, Dr. J. Neefjes
Department of Cell and Chemical Biology and
the Institute for Chemical Immunology
Leiden University Medical Center LUMC
Einthovenweg 22, 2333 ZC, Leiden (The Netherlands)

[c] Dr. S. Pujals,[+] Dr. L. Albertazzi
Department of Nanoscopy for Nanomedicine
Institute of Bioengineering of Catalonia (IBEC)
Barcelona Institute of Science and Technology
08028 Barcelona (Spain)
E-mail: lalbertazzi@ibecbarcelona.eu

[d] Dr. E. Bos, Dr. A. J. Koster
Department of Electron Microscopy, Leiden University Medical Center LUMC
Einthovenweg 22, 2333 ZC, Leiden (The Netherlands)

E-mail: a.j.koster@lumc.nl

[e] Dr. A. H. Meijer
Institute of Biology Leiden, Leiden University
Sylviusweg 72, 2333 BE, Leiden (The Netherlands)

[f] Dr. L. Albertazzi
Department of Biomedical Engineering and
Institute of Complex Molecular Systems
Eindhoven University of Technology
5600 MB Eindhoven (The Netherlands)

[+] These authors contributed equally to this work.

📖 Supporting Information and the ORCID identification numbers for the
authors of this article can be found under https://doi.org/10.1002/
cbic.201800230.

This has limited their use to bacterial strains for which these techniques are available.

In an effort to image the subcellular location of bacteria in host phagocytes, we recently reported an approach that allowed visualization of bacteria within the ultrastructural context of the host cells. We imaged BONCAT-labelled *E. coli* by using correlative light and electron microscopy (CLEM).[11] After sectioning frozen cell samples down to a thickness of 75 nm followed by an on-section copper-catalysed Huisgen cycloaddition (ccHc) reaction,[12] we imaged the resulting bioorthogonal labels by using confocal microscopy. Subsequent transmission electron microscopy (TEM) of the same section allowed the placement of the fluorescent signal within its ultrastructural context of the phagocytose.

If this approach could be extended to pathogenic species, it would provide a powerful tool to study the interaction of host phagocytes with intracellular pathogens. However, for the approach to be of use for unmodified strains, two major constraints relating to both BONCAT and CLEM have to be overcome. The first is the reliance on mutant tRNA/tRNA synthases for the incorporation of the bioorthogonal amino acids, compounded by the low overall signal in BONCAT-CLEM (stemming from the thinness of the samples). We hypothesized that metabolic hijacking approaches reported for *E. coli* auxotrophic strains[13] would need to be extended and optimized to allow sufficient label incorporation with nonauxotrophic bacterial species, thus ensuring their detection by CLEM. The second limitation is related to the CLEM imaging itself: whereas the resolution of the electron micrograph is of the order of 1 nm, that of fluorescence microscopy is limited by the Abbe diffraction limit of half the photon wavelength ($\lambda \approx 250$ nm),[14] resulting in a resolution gap between the two techniques.

Over the last few years, super-resolution imaging techniques have flourished,[15] breaking Abbe's law and allowing for resolution on the nanoscale. Herein, we describe an improvement on the BONCAT-CLEM methodology, namely, its combination with super-resolution microscopy. This will aid in overcoming the hurdles related to pathogen BONCAT-CLEM: the sensitivity and improved resolution of stochastic optical resolution microscopy (STORM)[16] on cryosections to bring the resolution of the fluorescent signals in closer alignment with TEM and to improve sensitivity of detection, allowing imaging of genetically unmodified pathogenic bacteria by CLEM.

Results and Discussion

One pathogen that would benefit from lifecycle studies using STORM-CLEM is *Salmonella enterica* Typhimurium (henceforth referred to as *S.* Typhimurium or *Salmonella*). This is a Gram-negative facultative intracellular pathogen that ensures its intracellular survival by secreting various effector proteins after uptake.[17] These modulate the maturation of the phagosome in which the bacterium resides to yield a parasitic vacuole suitable for its survival and replication.[18] To apply our STORM-CLEM to the imaging of *Salmonella,* we first assessed whether we could incorporate bioorthogonal amino acid analogues by using BONCAT to sufficient levels to allow ccHc detection of

bacterial proteome after uptake by phagocytes without affecting bacterial growth and infectivity. We optimized the incorporation of homopropargylglycine (Hpg) in vitro by using an in-gel fluorescence assay (Figure S1 in the Supporting Information) and observed detectable incorporation after pulsing with Hpg (0.04–4 mM) for 30 min. This was confirmed by flow cytometry (Figures 1 A and S2). BONCAT of a DsRed-expressing strain of *Salmonella*[19] showed no effect on DsRed expression levels in the presence of Hpg up to a concentration of 0.4 mM (Figure S2). Outgrowth experiments—for which growth rates were determined after Hpg pulses (Figure S3)—showed that growth rates recovered to ±90% within 1 h (after 30 min Hpg pulse). Recovery was longer (up to 3 h) with longer Hpg pulses.
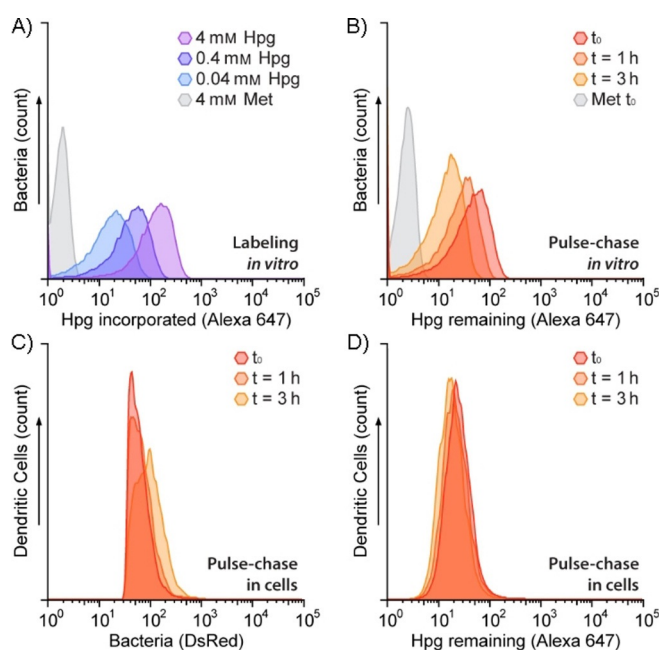
Figure 1. Flow cytometric analysis of Hpg–*S.* Typhimurium labelling and label persistence in vitro and in cells. A) *S.* Typhimurium were incubated with Met (4 mM) or Hpg (0.04–4 mM) before being subjected to fixation and ccHc with Alexa-647-azide. B) Label persistence was determined by incubating *S.* Typhimurium with 0.4 mM Hpg for 30 min and measuring the ccHc signal at the indicated times. Label persistence inside DC2.4 cells C) showing DsRed expression as a measure of the total number of bacteria and D) showing ccHc signal persistence over 0–3 h.

The evolution of Hpg-label density during division was also followed by using in-gel fluorescence (Figure S1) and flow cytometry[10] (Figures 1 B, S2, and S4). Detectable ccHc-mediated fluorophore introduction was still observed after 2 h of outgrowth ($\approx$2–6 divisions[20]). On the basis of these observations, the optimal conditions, balancing the strength of the signal and the impact on *Salmonella* growth, were chosen as 0.5 h pulse with 0.4 mM. However, it is important to note that even at these optimal concentrations it was not possible to achieve a homogeneous bioorthogonal/DsRed positive bacterial population, perhaps as a result of the loss of DsRed expression during the infection time course or because the Hpg expres-

sion conditions caused a reduction in the DsRed signal (Figure S2k).

We next determined whether infectivity was affected for the bioorthogonal *S.* Typhimurium. We incubated the aforementioned DsRed-expressing strain, grown with Met or Hpg, with bone-marrow-derived dendritic cells (BM-DCs)[21] for 30 min and assessed uptake and intracellular cell division by using flow cytometry.

By quantifying both the DsRed and bioorthogonal signals over time, bacterial cell divisions and label loss could both be detected. Hpg modification did not affect BM-DC uptake (Figure S4).The rate of DsRed expression after uptake in both Met- and Hpg-grown strains was equal, indicating no detectable impact of Hpg on intracellular survival or proliferation (Figures 1 C and S4). Furthermore, bioorthogonal ligation within BM-DCs showed no reduction in click signal, confirming our previous finding that nonstrained alkynes were stable in the phagolysosomal pathway[22] (Figures 1 D and S4).

Confocal microscopy of Hpg-grown DsRed–*Salmonella* revealed full colocalization of the DsRed signal with the bioorthogonal Alexa-488 signal (Figure 2), albeit weaker than that observed for Hpg-grown auxotrophic *E. coli* (B834),[11b] likely as a result of lower incorporation of Hpg in the presence of locally produced Met by the nonauxotrophic *S.* Typhimurium.[23] To quantify the colocalization of the two signals, we performed an automated statistical analysis[24] of the images by calculating the Manders coefficients,[25] M_1 and M_2, which reveal the degree of colocalization of DsRed to Alexa-488 and vice versa, respectively. At the optimum threshold, 73 and 85 % colocalization was obtained, respectively, highlighting subquantitative but high labelling efficiency of the bacteria.

We next assessed whether the fluorescence levels observed above were sufficient to allow BONCAT-CLEM in 75 nm sections. BM-DCs were again incubated with Hpg-*S.* Typhimurium and subjected to Tokuyasu sample preparation,[26] and this was followed by labelling with Alexa-488-azide by using a ccHc reaction. Confocal microscopy of the labelled cryosections revealed the fluorescence signal to be at the limit of detection

(Figure S5), rendering the approach unsuitable for imaging the phagocyte–*Salmonella* interaction, unless a signal enhancement step[27] with an anti-Alexa-488-antibody was used (Figure S6). Correlation of the fluorescence images and electron micrographs was performed by using nuclear 4′,6-diamidino-2-phenylindole (DAPI) staining in the fluorescence images and the morphological information obtained from the electron micrographs, and it showed that the Hpg-positive foci were located on intact bacterial structures as well as on smaller non-double membrane containing structures (Figure S6 d,e, yellow arrows).
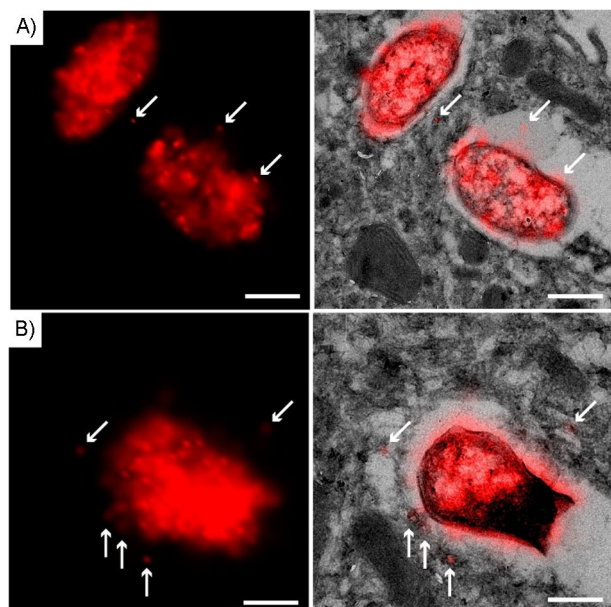
The resolution of the fluorescence signal limited the accuracy of correlation to approximately 250 nm.[14] Recently, the combination of fluorescent protein super-resolution imaging was combined with CLEM, and this allowed a tenfold improvement in the fluorescence resolution of fluorescent proteins.[28] By lowering OsO_4 concentrations during post-fixing and optimizing resin embedding, fluorophore quenching could be partially prevented. This sample preparation technique was reported with both PALM (photoactivated localization microscopy)[28a, 29] and STED (stimulated emission depletion) microscopy in combination with TEM[30] and scanning electron microscopy (SEM).[28b, 31] Of the various super-resolution imaging techniques, STORM offers higher spatial resolution and sensitivity[32] at the cost of longer acquisition times. Although this is a drawback for in vivo imaging, it presents no problem upon imaging fixed sections. The other limitation of STORM is the need to observe close to the glass surface owing to total internal reflection fluorescence illumination. The thinness of the cryosections (75 nm) makes the two approaches very compatible. We therefore selected STORM as a candidate technique to pursue the CLEM imaging of bioorthogonal groups. The two-step nature of bioorthogonal ligations also simplifies the STORM-CLEM workflow, because the fluorophore is introduced after the biological time course and sample preparation. The choice of fluorophore can therefore be made independently of the requirements of the biological experiment. The limited availability of dyes for STORM is thus circumvented.[33] We first deter-
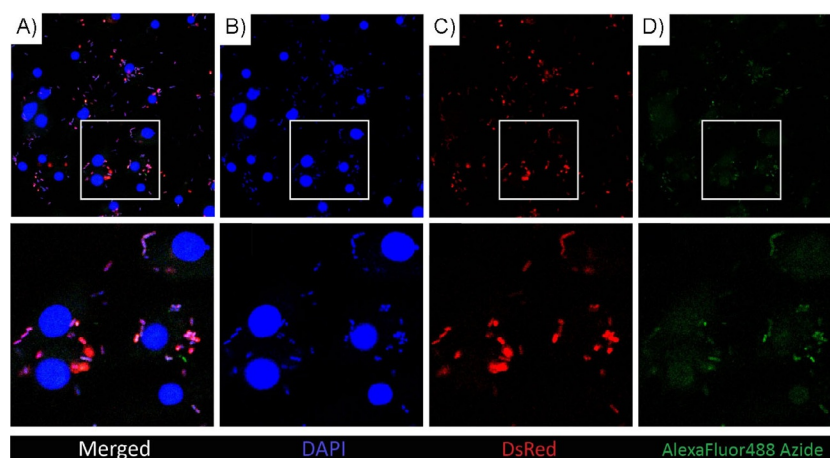
Figure 2. Confocal microscopy of BM-DCs incubated with Hpg–*S.* Typhimurium: BM-DCs were incubated with Hpg–*S.* Typhimurium expressing DsRed. After a 45 min pulse, cells were washed and fixed/permeabilized. Cells were subsequently labelled with Alexa-488-azide (green = Alexa-488) and DAPI. A) Merged channels, B) DAPI only, C) DsRed, and D) Alexa-488-azide; top: Low-magnification overview and bottom: high-magnification view of inset.

mined the limit of detection of STORM by imaging cryosections of bacteria grown in the presence of decreasing amounts of Hpg (Figures S7 and S8). Samples were cryosectioned, ccHc-ligated with Alexa-647-azide, and imaged by using standard catalase, glucose and glucose oxidase–containing buffer (GLOX) or other oxygen-consuming buffers, such as the OxEA buffer[34] supplemented with 30% glycerol to decrease drift during STORM image acquisition. The acquired STORM images of bacterial sections incubated with 0.4 or 4.0 mm Hpg revealed clear bacteria-sized regions (2300–400 nm × 180–280 nm) without the need for signal enhancement. Cells grown in the presence of 0.04 mm Hpg could be detected, but the signal was too low to allow full reconstruction of the bacteria.

We next used the STORM-CLEM approach to detect Hpg–*Salmonella* within BM-DCs (Figure 3). Both the accuracy and detection sensitivity of fluorescently labelled Hpg–*S.* Typhimurium were drastically higher for the STORM images than for the low-resolution confocal images. Subsequent visualization of the intracellular environment by electron microscopy showed that STORM had not damaged the phagocyte ultrastructures. Membranes were found to be intact, and no structural alterations were observed between regions of the sample subjected to STORM imaging relative to those not analysed by STORM. Organelles were readily recognizable on the basis of their distinct morphological appearances. Correlation of the STORM images showed that the bioorthogonal signals were primarily on the *Salmonella* bacteria or on small structures with a diameter of approximately 10–20 nm surrounding the parasitic vacuole.

Conclusions

This first example of super-resolution stochastic optical reconstruction microscopy (STORM)–correlative light electron microscopy (CLEM) by using bioorthogonal groups and its application to the study of host–pathogen interactions could thus be used to see non-genetically modified pathogens within their spatially detailed host environments. The sensitivity, compared to our method and those previously reported,[11b, 35] even allowed the detection of extracellular protein products. This opens up the possibility of imaging pathogens for which previous bioorthogonal noncanonical amino acid tagging (BONCAT) approaches were not efficient. The combination of STORM-CLEM with BONCAT, tRNA/tRNA synthetase mutants, or bioorthogonal cell-wall labelling will be valuable in studying the in vivo lifecycle of these pathogens.[7] Application of this technique to other areas in which bioorthogonal chemistry has been transformative would also add an extra dimension of ultrastructure to these fields.[36]

Conflict of Interest

The authors declare no conflict of interest.

Figure 3. Super-resolution N-STORM-CLEM image of a 75 nm cryosection of BM-DCs incubated with Hpg–*S.* Typhimurium. BM-DCs were incubated with Hpg–*S.* Typhimurium and were washed with phosphate-buffered saline to remove unbound/noninternalized *S.* Typhimurium. Cells were fixed and subjected to Tokuyasu sample preparation and cryosectioned into 75 nm sections. Sections were treated with Alexa-647-azide by using ccHc conditions (red). Left: Examples A) 1 and B) 2 of super-resolution N-STORM imaging of Hpg–*S.* Typhimurium. Right: Super-resolution CLEM images of the left-hand panels. Arrows indicate extraphagosomal signals. Scale bars: 250 nm.

[1] G. Mitchell, R. R. Isberg, *Cell Host Microbe* **2017**, *22*, 166 – 175.
[2] S. Pandey, T. Kawai, S. Akira, *Cold Spring Harbor Perspect. Biol.* **2015**, *7*, a016246.
[3] a) M. S. Siegrist, S. Whiteside, J. C. Jewett, A. Aditham, F. Cava, C. R. Bertozzi, *ACS Chem. Biol.* **2013**, *8*, 500 – 505; b) P. Shieh, M. S. Siegrist, A. J. Cullen, C. R. Bertozzi, *Proc. Natl. Acad. Sci. USA* **2014**, *111*, 5456 – 5461; c) G. W. Liechti, E. Kuru, E. Hall, A. Kalinda, Y. V. Brun, M. VanNieuwenhze, A. T. Maurelli, *Nature* **2014**, *506*, 507 – 510.
[4] a) B. M. Swarts, C. M. Holsclaw, J. C. Jewett, M. Alber, D. M. Fox, M. S. Siegrist, J. A. Leary, R. Kalscheuer, C. R. Bertozzi, *J. Am. Chem. Soc.* **2012**, *134*, 16123 – 16126; b) K. M. Backus, H. I. Boshoff, C. S. Barry, O. Boutureira, M. K. Patel, F. D'Hooge, S. S. Lee, L. E. Via, K. Tahlan, C. E. Barry, B. G. Davis, *Nat. Chem. Biol.* **2011**, *7*, 228 – 235; c) F. P. Rodriguez-Rivera, X. Zhou, J. A. Theriot, C. R. Bertozzi, *J. Am. Chem. Soc.* **2017**, *139*, 3488 – 3495.
[5] D. C. Dieterich, A. J. Link, J. Graumann, D. A. Tirrell, E. M. Schuman, *Proc. Natl. Acad. Sci. USA* **2006**, *103*, 9482 – 9487.

[6] A. Mahdavi, J. Szychowski, J. T. Ngo, M. J. Sweredoski, R. L. Graham, S. Hess, O. Schneewind, S. K. Mazmanian, D. A. Tirrell, *Proc. Natl. Acad. Sci. USA* **2014**, *111*, 433 – 438.

[7] a) M. Grammel, P. D. Dossa, E. Taylor-Salmon, H. C. Hang, *Chem. Commun.* **2012**, *48*, 1473 – 1474; b) M. Grammel, M. M. Zhang, H. C. Hang, *Angew. Chem. Int. Ed.* **2010**, *49*, 5970 – 5974; *Angew. Chem.* **2010**, *122*, 6106 – 6110; c) S. Lin, Z. Zhang, H. Xu, L. Li, S. Chen, J. Li, Z. Hao, P. R. Chen, *J. Am. Chem. Soc.* **2011**, *133*, 20581 – 20587.

[8] J. T. Ngo, J. A. Champion, A. Mahdavi, I. C. Tanrikulu, K. E. Beatty, R. E. Connor, T. H. Yoo, D. C. Dieterich, E. M. Schuman, D. A. Tirrell, *Nat. Chem. Biol.* **2009**, *5*, 715 – 717.

[9] A. G. Chande, Z. Siddiqui, M. K. Midha, V. Sirohi, S. Ravichandran, K. V. S. Rao, *Sci. Rep.* **2015**, *5*, 13430.

[10] R. Hatzenpichler, S. A. Connon, D. Goudeau, R. R. Malmstrom, T. Woyke, V. J. Orphan, *Proc. Natl. Acad. Sci. USA* **2016**, *113*, E4069 – E4078.

[11] a) D. M. Van Elsland, E. Bos, J. B. Pawlak, H. S. Overkleeft, A. J. Koster, S. I. Van Kasteren, *J. Microsc.* **2017**, *267*, 309 – 317; b) D. M. van Elsland, E. Bos, W. de Boer, H. S. Overkleeft, A. J. Koster, S. I. van Kasteren, *Chem. Sci.* **2016**, *7*, 752 – 758; c) D. M. van Elsland, E. Bos, H. S. Overkleeft, A. J. Koster, S. I. van Kasteren, *J. Chem. Biol.* **2015**, 8, 153 – 157.

[12] a) C. W. Tornøe, C. Christensen, M. Meldal, *J. Org. Chem.* **2002**, *67*, 3057 – 3064; b) V. V. Rostovtsev, L. G. Green, V. V. Fokin, K. B. Sharpless, *Angew. Chem. Int. Ed.* **2002**, *41*, 2596 – 2599; *Angew. Chem.* **2002**, *114*, 2708 – 2711.

[13] K. L. Kiick, D. A. Tirrell, *Tetrahedron* **2000**, *56*, 9487 – 9493.

[14] E. Abbe, *Arch. Mikrosk. Anat. Entwicklungsmech.* **1873**, *9*, 413 – 418.

[15] S. J. Sahl, S. W. Hell, S. Jakobs, *Nat. Rev. Mol. Cell Biol.* **2017**, *18*, 685.

[16] M. J. Rust, M. Bates, X. W. Zhuang, *Nat. Methods* **2006**, *3*, 793 – 795.

[17] C. M. Alpuche-Aranda, E. L. Racoosin, J. A. Swanson, S. I. Miller, *J. Exp. Med.* **1994**, *179*, 601 – 608.

[18] a) A. Haraga, M. B. Ohlson, S. I. Miller, *Nat. Rev. Microbiol.* **2008**, *6*, 53 – 66; b) C. G. Forest, E. Ferraro, S. C. Sabbagh, F. Daigle, *Microbiology* **2010**, *156*, 3689 – 3698; c) V. Krieger, D. Liebl, Y. Zhang, R. Rajashekar, P. Chlanda, K. Giesker, D. Chikkaballi, M. Hensel, *PLoS Pathog.* **2014**, *10*, e1004374; d) T. Scanu, R. M. Spaapen, J. M. Bakker, C. B. Pratap, L.-e. Wu, I. Hofland, A. Broeks, V. K. Shukla, M. Kumar, H. Janssen, J.-Y. Song, E. A. Neefjes-Borst, H. te Riele, D. W. Holden, G. Nath, J. Neefjes, *Cell Host Microbe* **2015**, *17*, 763 – 774.

[19] S. Méresse, O. Steele-Mortimer, B. B. Finlay, J. P. Gorvel, *EMBO J.* **1999**, *18*, 4394 – 4403.

[20] D. B. Lowrie, V. R. Aber, M. E. W. Carrol, *Microbiology* **1979**, *110*, 409 – 419.

[21] M. A. West, R. P. Wallin, S. P. Matthews, H. G. Svensson, R. Zaru, H. G. Ljunggren, A. R. Prescott, C. Watts, *Science* **2004**, *305*, 1153 – 1157.

[22] T. Bakkum, T. van Leeuwen, A. J. C. Sarris, D. M. van Elsland, D. Poulcharidis, H. S. Overkleeft, S. I. van Kasteren, *ACS Chem. Biol.* **2018**, *13*, 1173 – 1179.

[23] D. A. Smith, *Microbiology* **1961**, *24*, 335 – 353.

[24] J. W. D. Comeau, S. Costantino, P. W. Wiseman, *Biophys. J.* **2006**, *91*, 4611 – 4622.

[25] M. Manders, E. M. J. Verbeek, F. A. J. Aten, *J. Microsc.* **1993**, *169*, 375 – 382.

[26] K. T. Tokuyasu, *J. Cell Biol.* **1973**, *57*, 551 – 565.

[27] E. Bos, L. Hussaarts, J. R. T. van Weering, M. H. Ellisman, H. de Wit, A. J. Koster, *J. Struct. Biol.* **2014**, *186*, 273 – 282.

[28] a) E. Betzig, G. H. Patterson, R. Sougrat, O. W. Lindwasser, S. Olenych, J. S. Bonifacino, M. W. Davidson, J. Lippincott-Schwartz, H. F. Hess, *Science* **2006**, *313*, 1642 – 1645; b) B. G. Kopek, M. G. Paez-Segala, G. Shtengel, K. A. Sochacki, M. G. Sun, Y. Wang, C. S. Xu, S. B. van Engelenburg, J. W. Taraska, L. L. Looger, H. F. Hess, *Nat. Protocols* **2017**, *12*, 916 – 946.

[29] a) N. de Souza, *Nat. Methods* **2015**, *12*, 37 – 37; b) H. Suleiman, L. Zhang, R. Roth, J. E. Heuser, J. H. Miner, A. S. Shaw, A. Dani, *eLife* **2013**, *2*, e01149.

[30] a) S. Watanabe, A. Punge, G. Hollopeter, K. I. Willig, R. J. Hobson, M. W. Davis, S. W. Hell, E. M. Jorgensen, *Nat. Methods* **2011**, *8*, 80 – 84; b) K. A. Sochacki, G. Shtengel, S. B. van Engelenburg, H. F. Hess, J. W. Taraska, *Nat. Methods* **2014**, *11*, 305 – 308; c) S. Watanabe, J. Richards, G. Hollopeter, R. J. Hobson, W. M. Davis, E. M. Jorgensen, *J. Vis. Exp.* **2012**, e3995.

[31] a) B. G. Kopek, G. Shtengel, C. S. Xu, D. A. Clayton, H. F. Hess, *Proc. Natl. Acad. Sci. USA* **2012**, *109*, 6136 – 6141; b) B. G. Kopek, G. Shtengel, J. B. Grimm, D. A. Clayton, H. F. Hess, *PLoS One* **2013**, *8*, e77209.

[32] a) J. Tam, D. Merino, *J. Neurochem.* **2015**, *135*, 643 – 658; b) A. G. Godin, B. Lounis, L. Cognet, *Biophys. J.* **2014**, *107*, 1777 – 1784; c) L. MacDonald, G. Baldini, B. Storrie in *Membrane Trafficking*, 2nd ed. (Ed.: B. L. Tang), Springer, New York, **2015**, pp. 255 – 275; d) A. Oddone, I. V. Vilanova, J. Tam, M. Lakadamyali, *Microsc. Res. Tech.* **2014**, *77*, 502 – 509.

[33] G. T. Dempsey, J. C. Vaughan, K. H. Chen, M. Bates, X. W. Zhuang, *Nat. Methods* **2011**, *8*, 1027 – 10275.

[34] L. Nahidiazar, A. V. Agronskaia, J. Broertjes, B. van den Broek, K. Jalink, *PLoS One* **2016**, *11*, e0158884.

[35] a) J. T. Ngo, S. R. Adams, T. J. Deerinck, D. Boassa, F. Rodriguez-Rivera, S. F. Palida, C. R. Bertozzi, M. H. Ellisman, R. Y. Tsien, *Nat. Chem. Biol.* **2016**, *12*, 459 – 465; b) M. Scotuzzi, J. Kuipers, D. I. Wensveen, P. de Boer, K. C. Hagen, J. P. Hoogenboom, B. N. Giepmans, *Sci. Rep.* **2017**, *7*, 45970; c) S. R. Adams, M. R. Mackey, R. Ramachandra, S. F. Palida Lemieux, P. Steinbach, E. A. Bushong, M. T. Butko, B. N. G. Giepmans, M. H. Ellisman, R. Y. Tsien, *Cell Chem. Biol.* **2016**, *23*, 1417 – 1427.

[36] a) R. S. Erdmann, H. Takakura, A. D. Thompson, F. Rivera-Molina, E. S. Allgeyer, J. Bewersdorf, D. Toomre, A. Schepartz, *Angew. Chem. Int. Ed.* **2014**, *53*, 10242 – 10246; *Angew. Chem.* **2014**, *126*, 10407 – 10412; b) P. Mateos-Gil, S. Letschert, S. Doose, M. Sauer, *Front. Cell. Dev. Biol.* **2016**, *4*, 98.